SLAC-PUB-12695
July 2007

Effects of molecular interface modification in hybrid organic-inorganic photovoltaic cells

Chiatzun Goh, Shawn R. Scully and Michael D. McGehee[a)]

Department of Materials Science & Engineering, Stanford University, Stanford, CA 94305

ABSTRACT

We have systematically investigated the effects of surface modification of titania (TiO_2) in hybrid TiO_2/regioregular poly(3-hexylthiophene) (P3HT) photovoltaic cells. By employing a series of para-substituted benzoic acids with varying dipoles and a series of multiply-substituted benzene carboxylic acids, the energy offset at the TiO_2/polymer interface and thus the open circuit voltage of devices can be tuned systematically by 0.25 V. Transient photovoltage measurements showed that the recombination kinetics were dominated by charge carrier concentration in these devices and were closely associated with the dark current. The saturated photocurrent of TiO_2/P3HT devices exhibits more than a two-fold enhancement when molecular modifiers with large electron affinity were employed. The ability of modifiers to accept charge from polymers, as revealed in photoluminescence quenching measurement with blends of polymers, was shown to be correlated to the enhancement in device photocurrent. A planar geometry photoluminescence quenching measurement showed that TiO_2 substrates modified by these same molecules that accept charge quenched more excitons in regioregular P3HT than bare TiO_2 surfaces. An exciton diffusion length in P3HT as large as 6.5 – 8.5 nm

Submitted to Journal of Applied Physics

Work supported in part by US Department of Energy contract DE-AC02-76SF00515
SLAC, Stanford University, Stanford, CA 94025

was extracted. By measuring the external quantum efficiency (EQE) of working devices, it was found that all of the excitons that were quenched were accountable as extracted photocurrent. EQE was effectively increased from 5% to 10 – 14% with certain surface modifiers; consequently exciton harvesting was more than doubled. The use of Ruthenium (II) sensitizing dyes with good exciton harvesting property coupled with suppression of the recombination kinetics improved the efficiency of optimized bilayer TiO_2/P3HT devices from 0.34 % to 0.6 % under AM 1.5 solar illuminations. The implication of this work is directly relevant to the design of nanostructured bulk heterojunction inorganic-organic cells, in which efficient exciton harvesting and control of the recombination kinetics are key to achieving high efficiency.

---

a) Electronic mail: mmcgehee@stanford.edu

Subject-matter keywords: photovoltaic cells, organic, hybrid organic-inorganic, poly(3-hexylthiophene), P3HT, titania, TiO_2, molecular, surface, interface, modification, recombination, dipoles, protonation, dyes, bilayer, bulk heterojunctions.

I. INTRODUCTION

There has been tremendous development in the field of organic photovoltaic (PV) cells[1-7] and dye-sensitized solar cells (DSSCs)[7-10] as part of a continuous effort to realize low-cost solar cells. These excitonic solar cells[11] rely on the offset band energy[1-3] at a donor-acceptor heterojunction to split excitons.[12,13] Due to the small exciton diffusion length in typical organic semiconductors of 3 – 15 nm,[14-18] the most efficient organic solar cells have been based on blending the donor acceptor phases intimately together in so called "bulk heterojunction" structure,[2,3] such that all excitons can reach the interface before undergoing geminate recombination. Once the excitons are split, the charge carriers need to be collected by the external electrodes before they recombine at the interface. In bulk heterojunction PV cells, the large interfacial area between the donor-acceptor pair inherently increases the cross section for charge recombination and consequently increases device dark current. There is increasing evidence of the formation of geminate pairs upon exciton separation in some devices,[19-21] which requires engineering of the interface energetics to improve the yield of fully separated electron and hole carriers under operating condition. By optimizing the interface energetics, the exciton splitting can be engineered efficient, while the back recombination of split carriers can be suppressed. Therefore, the study and application of interface engineering is essential towards improving excitonic solar cells performance.

Interface modification can have many effects on a PV cell. Molecular interface modifiers (IM) can impart a dipole at the donor-acceptor interface and shift the interface energy offset upon attachment.[22-24] Besides affecting the energy levels of the donor-acceptor pair, the IMs' molecular orbitals form electronic states at the interface, which

may block or mediate forward charge transfer or reduce back charge recombination. Furthermore, IMs are known to passivate inorganic surface states by chemically interacting with surface dangling bonds,[25,26] thus changing the surface energetics. By modifying the physical and chemical properties of a surface, the IMs also affect the interfacial interaction with a material, for example giving rise to different growth modes or morphologies of organic semiconductors.[27,28] Lastly, IMs can act as energy acceptors if their absorption spectrum overlaps with the photoluminescence of an emitter in close proximity.[29]

The combination of metal oxide (e.g. titania, tin oxide, zinc oxide) and conjugated polymer is an attractive donor-acceptor pair candidate in excitonic solar cells.[30-33] In these hybrid inorganic-organic PV cells, the inorganics can be individually structured before the organic phase is incorporated to form bulk heterojunction PV cells.[34,35] The flexibility to pattern these metal oxides separately makes it easier to fabricate ordered bulk heterojunction[36-39] and conveniently allows the interface modification step to be included before the organics are deposited. The ability to tune the interfacial properties while keeping the same donor-acceptor materials provides for a means to systematically study the effect of interface modification. Modification of organic-inorganic interfaces using molecular materials is fitting, as the surface of metal oxides guarantees well-situated reactive sites for molecular attachment. Although substantial effort has been directed towards improving the efficiency of hybrid PV cells, the focus was on the combination of different materials as donor-acceptor pair and how best to optimize nanoscale phase separation,[31,32,35,38,39] while little work has been done to investigate the donor-acceptor interface.[22,38,40]

For this study, we modified the interface in titania (TiO_2)/regioregular poly(3-hexylthiophene) (P3HT) PV cells by attaching molecules to TiO_2 that bind via carboxylate bonds. We tuned the interfacial energy level offsets by forming interfacial dipoles with both a series of para-substituted benzoic acids (Fig. 1a) and a class of benzene carboxylic acid molecules (Fig. 1b). The change in energy level offset resulted in a correlated change in the dark current of the PV device and the open circuit voltage (V_{oc}). Transient photovoltage (TPV) measurements revealed the recombination kinetics in these devices, which explains the difference in dark current. IMs with large electron affinity tend to yield larger photocurrent by at least two-fold compared to an unmodified cell. Photoluminescence (PL) quenching measurement of blends of IMs with P3HT showed a clear correlation of the IM's ability to quench excitons in P3HT and the enhancement in device photocurrent. A planar geometry PL quenching measurement showed that TiO_2 substrates modified by these same molecules that possess large electron affinity quenched more excitons in P3HT than bare TiO_2 surface. This enhanced exciton harvesting results in an extracted exciton diffusion length (L_d) of 6.5 – 8.5 nm for P3HT. The measured external quantum efficiency (EQE) of working devices accounted for all the photocurrent predicted based on the number of quenched excitons, with EQE increasing from 5% to 10 – 14% with surface modifications. We further employed a class of red Ruthenium (II) dye molecules (Fig. 1c) with good exciton harvesting property and concomitantly controlled the interfacial recombination kinetics to improve the efficiency of optimized bilayer TiO_2/P3HT devices from 0.35 % to 0.6 % under AM 1.5 solar illuminations. An amphiphilic Ru (II) dye showed great promise as an IM

candidate to be used in bulk heterojunction devices as it suppresses charge carrier recombination while retaining efficient exciton harvesting.

II. EXPERIMENT

Contact angle measurements were performed on a Ramé-hart 100 contact angle goniometer. Atomic force microscope (AFM) measurements were made with a multimode Veeco AFM using Tap150 probes (Nanodevices). PL quenching measurements were taken with samples loaded in nitrogen sealed chamber. PL excitation was provided by a 512-nm Spectra-Physics Stabilite 2017 argon ion laser at an incident angle of ~ 30° from the film normal. The PL was collected at the normal angle with an Acton Research Spectra Pro 500i spectrometer coupled with a CCD camera. The TiO_2 films used in PL measurements were made thin (~ 5 - 8 nm) to ensure a negligible effect from optical interference.[29]

All chemicals were purchased from Aldrich except the Ru(II) dyes, which were purchased from Solaronix SA. All chemicals were used as received except P3HT, which was purified by Soxhlet extraction using hexane and then chloroform before use. Sol-gel TiO_2 films were prepared either on glass or fluorine-doped tin oxide (FTO) substrates (AFG Industries, Inc., 100 Ω/square). Substrates were cleaned by ultrasonication in Extran-100 surfactant, acetone, isopropanol and deionized water. TiO_2 films were made by mixing 100 part ethanol, 2.5 part deionized water and 1 part concentrated hydrochloric acid by volume together. 1 part of titanium tetraethoxide was then mixed with 8 part of ethanol solution. The mixture was stirred for at least 15 minutes and filtered through a 0.45 μm filter. The sol-gel solution was spin coated onto substrates at 2000 – 3000 rpm.

Films were condensed in an oven at 120 °C overnight and calcined at 450 °C for 1 h to achieve typical thickness of 70 – 90 nm. To make 6 – 8 nm thick TiO_2 films for PL quenching measurements, a dilute sol-gel solution was prepared by mixing 0.1 g of titanium tetraethoxide with 10 g of ethanol solution.

The surface of TiO_2 films were modified by immersing them for 2 – 3 hrs in (i) 1 mM benzoic derivative solution in acetonitrile, (ii) 0.3 mM carboxylic acid benzene solution in acetonitrile or (iii) 0.1 mM N3 in ethanol solution or 0.1 mM N719 or Z907 in 1:1 acetonitrile:t-butylalcohol solution. The films were thoroughly rinsed in 3 sets of fresh solvent (~ 2 mins total) and blow dried with nitrogen. t-butylpyridine (TBP) treatment was done by immersing substrates in TBP for 15 minutes with a subsequent ethanol rinse. The films were then moved into a nitrogen-purged glove box for subsequent deposition of polymer films and top silver (Ag) electrodes. P3HT films were spin-coated from tetrahydrofuran (THF) solutions. The Ag electrodes were thermally deposited in a chamber with pressure less than 1 x 10^{-6} Torr. Typical device area was ~0.05 cm^2. Finished devices of the structure FTO/TiO_2/(with or without) interface modifier/P3HT/Ag were annealed on a hot plate in an inert atmosphere at 130 -140 °C for 4 – 8 hours. Subsequent characterization and measurements were all done in the glove box.

Current-voltage (J-V) curves of devices were obtained with a Keithley 2400 source measure unit. Solar illumination was provided by a Spectra Physics 300W solar simulator equipped with an AM 1.5G filter. The light intensity was calibrated with a Newport 818SL silicon photodiode. The calculated spectral mismatch factor of 0.78 for P3HT is included in all reported efficiencies here. Once intensity was calibrated, a UV-

filter with a cutoff of 400 nm was placed in front of the cells to avoid optical excitation of the TiO_2. EQE measurements were obtained by illuminating devices with an expanded and uniformly collimated 512-nm Spectra-Physics Stabilite 2017 argon ion laser beam, whose intensity was monitored. Photocurrent action spectrum was obtained by illuminating the device with a scanning monochromatically-selected tungsten lamp that was chopped with a Scitec optical chopper. The photocurrent was monitored with a Stanford Research SR830 lock-in amplifier.

For the TPV experiment,[41] the devices were held at a certain steady state V_{oc} by illuminating from the solar simulator with adjustable intensity, while a frequency doubled Nd:YAG laser (λ = 532 nm, 5-7 ns FWHM) supplied the pulse beam for the transient photovoltage with a repetition rate of 11 Hz. A Tektronix TDS1012 digital oscilloscope was used to record the photovoltage decay transient. The transient photovoltage ΔV was kept below 10 mV to ensure a small perturbation to the steady-state V_{oc}.

III. RESULTS AND DISCUSSION

A bilayer TiO_2/P3HT cell configuration was chosen for this interface modification study because the planar heterojunction between TiO_2 and P3HT simplifies device modeling, analysis and fabrication. The use of layered device not only negates complicated issues related to bulk heterojunctions such as pore filling, phase segregation and charge collection, but also keeps the optical interference profile similar between devices provided the same layer thicknesses are used.[14,42] Insights attained from studying a planar system are directly applicable to bulk heterojunction systems, whose nanostructured inorganic phase can be similarly modified with IMs.

Figure 1a shows a schematic of a bilayer device. FTO is the electron collecting electrode, while the annealed Ag electrode (which we believe has Ag_2O at the surface) collects holes. P3HT is the best polymer that has been used in combination with acceptors like PCBM and TiO_2 in bulk heterojunction PV cells.[4,6,32,33] Its hole mobility of > 10^{-4} cm^2/Vs in the direction perpendicular to the substrate,[43] the direction pertinent for photocarrrier extraction, allows for large photocurrent to be transported without encountering space charge limited current.

Figure 1 shows the IMs used in this study. Three classes of molecular modifiers binding via carboxylate bonds were employed: (i) para-substituted benzoic derivative acid derivatives with different substituent group that vary the dipole moment[22,40,44,45] (Fig. 1a), (ii) benzene carboxylic acid molecules with varying number of carboxylic acid groups (Fig. 1b), and (iii) three Ru(II) red dyes used frequently in DSSCs, which are N3 dye,[10] N719 dye[46] and Z907 dye[47] or "hydrophobic dye" (Fig. 1c). Abbreviations are used to describe the molecules in the rest of this paper. For example, $–NO_2$ and –CN denote nitrobenzoic acid and cyanobenzoic acid, -TRI and -TETRA denote benzene tricarboxylic acid and benzene tetracarboxylic acid modifications.

To show that the IMs were bound to the surface of TiO_2, contact angle measurements were performed (not shown). A water drop on a bare TiO_2 surface, as calcined or after being rinsed with solvents like acetonitrile and THF, showed a contact angle of 0°. The water wet the bare TiO_2 surface completely due to its hydrophilicity. Upon coating with any IMs, the TiO_2 surface showed a non-zero contact angle. The organic IMs lowered the surface energy to different extents.

The difference in binding constants to TiO_2 and molecular sizes of the IM affects surface coverage. Kruger et. al showed that even though the attachment groups of the molecules with $–NO_2$ and $–OCH_3$ have different acidity, the surface concentration of adsorbed $–NO_2$ and $–OCH_3$ on TiO_2 at monolayer coverage was similar with surface area per molecule of ~ 0.3 nm^2.[22] On the other hand, the area occupied by N3 molecules at full monolayer coverage was found to be 1.65 nm^2 due to its larger molecular size.[10] Note that a monolayer coverage of a particular type of modifiers does not necessary mean perfect coverage, as additional coadsorption of smaller molecules[45] and intercalation of solvent molecules can be possible.[44]

A. Band edge shift

One effect the IMs have is to change the band offset at the interface by forming a layer of dipoles. Depending on the chemical nature of the IM, there can be two contributions: (i) the molecular dipole, which depends on the electron withdrawing and donating nature of the atoms across the molecular structure,[22] (ii) the protonation of the TiO_2 surface stemming from the dissociative adsorption of the carboxylic acid group to form a carboxylate bond, in which the positive charge of the proton on the surface and the negative charge on the carboxylic group forms an interfacial dipole.[23,24] The TiO_2 band edge has been shown to shift according to the Nernstian potential dependence of 60 mV per pH unit in solution.[48]

1. Band edge shift due to molecular dipoles

The use of molecular dipoles to adjust the work function of semiconductors or metals in general has been widely investigated.[40,49] Much of the work was directed towards improving charge injection from metals into organic materials in organic light emitting diodes and PV cells.[40,50,51] There are few reports of tuning the electron transfer kinetics and mechanism at a heterojunction interface, and even those were directed at DSSCs.[22,45]

We utilized the class of para-substituted benzoic acids investigated previously[22,40,44,45] but included two more derivatives, aminobenzoic acid and fluorosulfonyl benzoic acid. Depending on the specific functional group substituted at the para position, the IMs form a dipolar layer with varying dipole direction and strength. Table I tabulates the dipole moments of these molecules. The left column set was obtained from literature[52] for the corresponding substituted benzene without the carboxylic group, while the right column set was simulated[53] using density functional theory for the whole structure including the carboxylic group. As carboxylic group forms a chelating group to Ti(IV) acting like an ester-type linkage, which causes it to be less electron-withdrawing, the dipole moments of adsorbed molecules are expected to fall somewhere between those two sets.

This dipolar layer, when attached to the TiO_2 surface, induces a step in the local vacuum level due to the electric field across this layer (Fig. 2). The work function and the band edge of the TiO_2 surface are changed by $e\Delta V$, where ΔV is the magnitude of surface potential change and can be calculated from Poisson's equation to be:

$$\Delta V = \frac{N_s \mu \cos\theta}{\varepsilon_r \varepsilon_0} \qquad (1)$$

and N_s is the surface dipole concentration, μ is the dipole moment, θ is the angle to which the dipole makes to the surface normal, ε_r is the dielectric constant, and ε_0 is the permittivity of free space. A linear relationship between the work function change of TiO_2 and the dipole moments of these para-substituted benzoic acid derivatives was determined previously using a Kelvin probe.[22,44]

Figure 2 illustrates schematically the energy band diagram for flat band conditions of a bilayer TiO_2/polymer system with and without a dipole sheet between them. Figure 2a shows that when the dipole is directed towards the TiO_2, the band edge potential of TiO_2 shifts away from the local vacuum level of the polymer. Thus the effective gap between the conduction band (E_c) of TiO_2 and the highest occupied molecular orbitals (HOMO) of polymer reduces when compared to unmodified TiO_2 in Figure 2b. If the dipoles are pointing away from titania, the band edge of titania shifts closer to the vacuum level of the polymer, and the gap between E_c and HOMO increases (Fig. 2c). Because the typical photocarrier concentration of 10^{15} - 10^{16} cm^{-3} under usual illumination is smaller than the valence and conduction edge density of states, the V_{oc}, the split between the electron and hole quasi Fermi levels under illumination, is limited by the effective E_c – HOMO gap. The presence of a dipole layer changing the effective E_c – HOMO gap consequently affects the maximum attainable V_{oc}. Although the maximum V_{oc} attainable is thermodynamically limited by this gap, the actual V_{oc} observed critically depends on the recombination kinetics of charge carriers (Sec. D). Figure 2 is drawn such that flat band condition is assumed to be close to the open circuit condition, although we acknowledge the existence of diffusion photocurrent away from the heterojunction causes the band to slope slightly at open circuit condition.[11,54]

The TiO_2 samples modified with various molecular dipoles were used to fabricate bilayer TiO_2/P3HT devices. Figure 3 shows the device characteristics in the dark and under AM 1.5 illumination. A thick polymer layer (~160 nm) was used to improve the device yield and to obtain more reproducible dark current, which is affected by shunting when the polymer film is thin. Any difference in the J-V characteristics shown in Figure 3 arises from the existence of the molecular dipoles. The dark J-V curves in Figure 3a have similar shapes, and differ only by an offset along the voltage axis. The amount of voltage shift between the devices of ~ 250 mV has been previously observed in solid state DSSCs.[22]

The V_{oc} of P3HT devices is plotted against the calculated dipole moments of the molecular dipoles in Figure 3c. V_{oc} correlates very well with the dipole magnitude. Dipoles pointing at TiO_2 decreased V_{oc} by as much as 0.2 V, whereas dipoles pointing away from TiO_2 only increased V_{oc} by at most 0.03 – 0.05 V. The small increment in V_{oc} with dipoles pointing away from titania is possibly due to the opposite dipole contribution from protonation effect of the carboxylic acid group (Sec. A.2). In Figure 3c, this protonation contribution, determined from the vertical difference between the V_{oc} of the unmodified cell and the dashed line, is found to be ~ 0.06 – 0.07 V. The relative V_{oc} change with different molecular dipoles is reproducible, though the absolute V_{oc} between batches of films can vary by ± 30 mV. If we assume a previously measured N_s of 3 x 10^{18} m^{-2} and ε_r = 5.3 [22,44] in Eq. 1, a 0.85 V shift of the V_{oc} is expected with $–NO_2$ modification if the dipoles are oriented normal to the surface. The reduced magnitude of V_{oc} change with dipole moment in a real device is attributable to different orientation of the dipoles in contact with polymers,[55] a higher effective ε_r or a lower N_s.

That the trend of V_{oc} change and the dark current translation is correlated to the dipole moments of the IM strongly suggests that the main effect of the dipole is to change the energy offset at the TiO_2/polymer interface. There is no evidence of the IMs acting as physical tunneling barrier that suppresses recombination. The recombination kinetics difference is thus dominated by the energy offset at the interface. When the E_c – HOMO gap is smaller, the electron concentration in TiO_2 and hole concentration in P3HT are higher at a given voltage. Higher carrier concentration results in faster charge recombination rate and higher dark current. The earlier turn-on of dark current consequently results in a lower V_{oc}.

The short circuit current (J_{sc}) in these devices shows an interesting trend (Fig. 3b, c), in which an enhancement of ~2x was obtained using IMs with strong dipoles pointing towards TiO_2, which are $–NO_2$, -CN and $–SO_2F$. These same molecules have large electron affinity due to the strong electron-withdrawing substituted functional groups. Their role in accepting charges from polymer will be described in Section C. For comparison, lowest unoccupied molecular orbital (LUMO) values of ~ 3.0[56,57] and ~ 4.0 eV[58] are reported for benzoic acid and $–NO_2$ respectively.

2. Band edge shift due to protonation of titania

Acid-base interactions arising from the anchoring of the carboxylic acid group to TiO_2 affects the band edge of TiO_2 by protonating it and forming an interfacial dipole layer. The benzoic acid derivatives with one functional group contributed to the band edge shift this way (Sec A.1). However as the surface density of these carboxylic functional groups increases, the effect should be more pronounced. A class of multiply-

substituted benzene carboxylic acid molecules, shown in Figure 1b, was used. This class of molecules has increasing number of functional groups for protonation with varying pKa. Since their molecular dipoles are small compared to the para-substituted benzoic acid derivatives, the interfacial dipoles need to be mainly considered. The change in band edge due to this protonation effect is equivalently described by Figure 3a.

Figure 4b shows that IMs with more protonating groups result in lower V_{oc}. This trend is expected from the increasing protonation of the TiO_2 surface. The V_{oc} was not changed going from TETRA-substituted to HEXA-substituted molecules, suggesting the active number of anchoring groups saturates. Saturation of binding groups could be due to depletion of active sites on the TiO_2 surface or the surface pH dictating a certain number of dissociative carboxylic acid groups. The molecules not only bind edge-on, but can absorb face-on, potentially increasing the number of functional groups participating in the binding.[25] Unfortunately, we do not have more information about the absorption of this class of molecules.

Figure 4a shows that the shift in dark current causes a similar shift in V_{oc} observed under illumination (Fig. 4b) and can be similarly justified by the explanation given in Section A.1 on the increase in dark current with decreasing Ec-HOMO gap. Interestingly, the photocurrent with this class of IMs also increases with more electron withdrawing carboxylic groups, or in another words, larger electron affinity.

B. Ru(II) dyes modification

The third class of molecular IMs employed is the class of Ruthenium (II) dyes commonly used in DSSCs (Fig. 1c). These Ru(II) dyes posses suitable LUMO levels and

exhibit binding to TiO_2 that allow rapid electron transfer (< 50 fs)[10] to TiO_2. The LUMO levels (~ 3.95 eV)[59] also sit between the LUMO of P3HT (~ 3.0 eV) and the E_c of TiO_2 (~ 4.2 eV) and can possibly mediate charge transfer from the polymer to TiO_2. The energy levels of the three-layer system are such that the electron travels in one direction from the polymer to TiO_2 via the IM but is potentially inhibited from recombining with the polymer. These Ru(II) molecules possess a similar density of carboxylic acid group as the multiply-substituted benzene carboxylic acid molecules (Sec. A.2), thus a band edge shift in the TiO_2 of similar magnitude (~0.2 V) is expected upon attachment of these molecules. These molecules also possess small molecular dipoles resulting from the spatial asymmetry of the HOMO and the LUMO.[10]

The three Ru(II) dyes investigated as IMs are respectively N3, N719 and Z907. N3 is the most common dye used in DSSCs and exhibits fast electron transfer to TiO_2 upon photoexcitation.[10] N719 dye is similar in most aspects to N3 except the hydrogen of two of the carboxylic groups is substituted with tetrabutylammonium (TBA). This less protonated N719 dye resulted in an E_c closer to the vacuum level and showed higher V_{oc} when used in DSSCs.[23,46] Z907 dye is attractive because its amphiphilic nature improves interactions with polymers[47,60] and its alkyl chain is known to inhibit recombination and improve V_{oc}.[38,61]

Figure 5a plots the dark current of devices with these dye modifications. Figure 5b shows that all surface modifiers except for the Z907 dye reduced the V_{oc}. The reduction in V_{oc} is due to the protonation of the TiO_2 by the carboxylic acid. The N3-modified device showed the lowest V_{oc}, but if N719 with fewer carboxylic groups was used, the V_{oc} was increased by ~ 60 mV. In addition, we also employed the additive tert-

butylpyridine (TBP), which is known both to shift the band edge of TiO_2 upwards due to its basicity and to physically plug voids at the interface at the molecular scale, to increase the V_{oc}.[62,63] For both N3 and N719-modified titania, TBP increased the V_{oc} by another ~60-70 mV. All these shifts in V_{oc} are consistent with the picture of band edge shift due to interfacial dipoles. Interestingly, the hydrophobic dye Z907 actually enhanced the V_{oc}, even though the attachment of the molecules is achieved similarly through carboxylate groups. This is not surprising considering that that Z907 is known to slow down the recombination kinetics in solid state DSSCs[61] and zinc oxide/polymer devices.[38] Its 9-carbon alkyl chain has been credited for forming charge carrier recombination barrier.[61]

Figure 5b shows the photocurrent curves for the same devices. N3 and N719 dyes were found to enhance J_{sc} by ≥ 2x, while Z907 increased it by 60-70%. The photocurrent enhancement could not come from the sensitization effect of the dyes, because the absorption of a monolayer of these dyes is negligible. Photocurrent action spectra of these devices in Figure 5c show that there is no contribution beyond the adsorption edge of P3HT even though the dyes absorb out to 800 nm.[38] When normalized, the photocurrent action spectra in Figure 5c overlay on each other and match the absorption spectrum of P3HT. Section C explains that this enhanced J_{sc} originates from higher exciton quenching when TiO_2 is modified with the dyes

The N3 and N719-modified devices gave rise to slightly different enhancement, probably due to the different electronic coupling at the TiO_2/dye or dye/polymer interface. An interesting observation is that upon treatment with TBP, both N3 and N719 devices retained similar J_{sc}. This suggests that there is not always a tradeoff between J_{sc} and V_{oc}. In the case of Z907 modification, both J_{sc} and V_{oc} actually improved. Therefore, the

explanation of TiO_2 band edge shift increasing the driving force for forward charge transfer, which ultimately increases the charge transfer yield, is not applicable.

The lesser photocurrent enhancement from Z907 dye is intriguing. With similar LUMO levels and charge transfer property as the other two Ru(II) dyes, Z907 is expected to behave similarly. The uniqueness lies in its alkyl chains. At the same time that these insulating segments slow down charge carrier recombination and increase V_{oc}, the forward charge transfer from the polymer to the TiO_2 is also partially inhibited by the extending alkyl chains. This slower forward charge transfer rate may explain the smaller J_{sc} enhancement. Z907 is an attractive IM candidate in nanostructured metal oxides/polymer devices because it potentially imparts slow recombination kinetics to offset large recombination interface to maintain large V_{oc} and fill factor. A recent work also showed the concomitant benefit of using Z907, which is to increase the incorporation of P3HT in nanostructured template.[60]

C. Models for increased photocurrent yield

The modifications with all three groups of IMs resulted in enhanced photocurrent, by > 2x in some cases. We discussed earlier that the ability of IM to accept electrons from the polymer is closely linked to the enhanced photocurrent in devices. The charge accepting ability was revealed in a PL quenching experiment probing blends of P3HT with 2.5 mol % IM spun from THF solutions (not shown). The PL of P3HT is quenched in the vicinity of electron acceptors. IMs that enhance device photocurrent were consistently found to accept charges from P3HT.

The exact nature of exciton quenching by the IM is expected to differ in a blend compared to a monolayer on a flat surface. The quenching by a monolayer of IM attached onto TiO_2 is more relevant to working PV devices. By comparing the PL intensity of a polymer film on a planar quenching substrate and a non-quenching substrate for a range of polymer film thickness, the exciton diffusion length (L_d) can be determined.[64-66] Glass was used as the non-quenching substrate, while a thin layer of TiO_2 coated on glass with or without IM was the quenching substrate. Thin TiO_2 (~5 – 8 nm) was used to ensure a negligible effect from optical interference.[29,65] The variation in polymer film thickness spun on different modified TiO_2 surface was usually ± 1 nm. Film thickness was determined from the optical density.

Figure 6a shows the PL quenching as a function of P3HT film thickness. When deposited on bare TiO_2 or $–NH_2$ modified TiO_2, P3HT exhibits some quenching at large thickness, but the quenching never approaches 100% as its thickness is reduced.[64] This lack of complete quenching is unexpected because in very thin film of polymers ($d < L_d$), all the excitons should be able to diffuse to the quenching interface. For thin films where the absorption is assumed to be linear with thickness, the quenching profile follows:[66]

$$PL_{quenching} = \frac{L_d[1-\exp(-2d/L_D)]}{d[1+\exp(-2d/L_D)]} \qquad (2)$$

We extracted an L_d by fitting data to Eq. 2 to allow for comparison between the data sets. Figure 6a shows that when P3HT was deposited on $–NO_2$ modified TiO_2, the PL quenching is about twice as high compared to that on bare TiO_2 at large thickness and approaches 100% with decreasing film thicknesses. When the TiO_2 was modified with N3 dye, a slightly higher quenching was observed. The L_d extracted for $–NO_2$ modified and N3-modiifed substrates are 6.5 and 8.5 nm respectively. It is observed that among

other IMs used, only those with large electron affinity result in higher PL quenching. A similar L_d value for P3HT of 9 nm measured using triplet-triplet annihilation method was recently reported by I.D.W. Samuel.[67]

To see if the difference between the PL quenching magnitudes observed on bare and modified TiO_2 was due to difference in polymer film roughness, we performed AFM measurements. AFM micrograph of a 3.3 nm thick P3HT film on the different substrates showed that the polymer film covered the TiO_2 surfaces completely and exhibited similar surface Rms roughness of 0.4 – 0.45 nm (not shown). For comparison, the surface roughness of bare TiO_2 is only 0.27 nm. There was no polymer surface roughness difference to explain the PL quenching difference.

To prove that there is no diffusion of these IMs into the polymer causing PL quenching, we accounted for all the quenched excitons in photocurrent. Figure 6b shows EQE measurements of sufficiently thick P3HT (160 nm) bilayer devices. At this film thickness, the optical interference effect is negligible and the absorption profile follows Beer's Law. For a given L_d and a flat quenching surface and neglecting the reflectance loss, the EQE is expected as:[65,68]

$$EQE = \frac{L_d \alpha}{(1 + L_d \alpha)} \qquad (3)$$

The absorption coefficient, α, at 512 nm for P3HT is 1.9 x 10^5 cm^{-1}. The J-V curve for the unmodified cell shows saturated photocurrent with increasing reverse bias, indicating that geminate recombination is not a bottleneck and any photocurrent enhancement is not due to the competition between recombination and charge extraction. Experimentally, the EQE obtained on $–NO_2$ device is twice that on the unmodified cell, and the EQE of ~10 % at 512 nm is expected for L_d of 6.5 nm. Similarly the EQE value of ~14%

obtained for N3-modified device matches the value predicted from a 8.5 nm L_d. Therefore, diffusion of a monolayer of the surface modifiers cannot possibly account for the enhancement in PL quenching. The enhancement indeed originated from more excitons being split and they are accounted for as photocurrent.

Another effect that must be considered when using N3 dye is the energy transfer from P3HT to the dyes.[29,65] The rate of Förster transfer from P3HT to a 2-D sheet of N3 dye, calculated from the Förster equation, was estimated to be competitive with bulk diffusion only at a distance < 1 nm from the acceptors.[65] This mechanism also cannot account for the large enhancement in PL quenching.

We propose that there is non-perfect electronic coupling between the polymer and bare TiO_2. For example, the side chains of polymer can prevent the excitons from getting right next to the TiO_2 interface, or not all surface sites on bare TiO_2 are active as charge acceptors. The surface modifiers in this case can mediate charge transfer from the polymer to TiO_2 if the LUMO level is suitable for accepting electrons. The IMs attach themselves through chemical bonding such that they are physically next to the TiO_2, potentially providing a good electronic coupling. Experimentally, whenever IMs with high electron affinity were employed, higher J_{sc} was observed. The charge transfer yield is a product of the electronic coupling between the IM with TiO_2 and that between the polymer and the IM. Interestingly, Ru(II) dyes, which are known to transfer electron to TiO_2 effectively, enhanced J_{sc} the most. The origin of imperfect exciton quenching of P3HT on bare TiO_2 is under investigation.

The observation of enhanced exciton quenching on certain modified TiO_2 surface is significant. Previous studies assume that the TiO_2 surface is a perfect quenching

interface. This assumption was made because some experiments had shown that the exciton lifetime in conjugated polymer was significantly shortened in the presence of TiO_2. The lifetime of MEH-PPV has been shown to reduce from 300 ps to <10 ps.[31] and another work showed < 100 fs.[69] That of the oligomeric thiophene was shortened from 230 ps to < 6 ps.[70] This indicates that the charge transfer from polymer to bare TiO_2 can be very fast. Further improvement in the forward charge transfer rate cannot improve exciton splitting significantly. It is likely that IMs with suitable LUMO levels mediate charge transfer from P3HT to TiO_2, thereby bypassing some barriers and improving exciton harvesting. There should be relevance of the IM's LUMO participation in the charge transfer process as excitons encounter the IM prior to TiO_2.

D. Transient photovoltage measurement of recombination kinetics

In section A and B, the dark current of PV devices was compared to understand how the V_{oc} changes with interface modification. It was argued that the dark current is higher at a fixed voltage if the Ec – LUMO gap is smaller due to higher electron and hole carrier concentration. The recombination rate in operating devices was determined by making transient photovoltage measurement (TPV) measurements.[41] In a TPV measurement (Fig. 7a), devices are held at a steady state V_{oc}, the magnitude of which is adjusted by varying the intensity of a bias lamp. A pulsed light creates a small perturbation to the V_{oc} by transiently generating electrons and holes. At V_{oc}, these additional carriers (photovoltage) decay with the lifetime determined by the rate of charge carriers recombining across the heterojunction interface. Figure 7b shows a typical TPV curve. The decay curve can be fitted to a monoexponential decay to extract

a characteristics lifetime, τ. The effective recombination rate, k_{rec}, is $1/\tau$. If recombination is assumed to be second order bimolecular, the recombination rate

$$\frac{d(n)}{dt} = -B \cdot n \cdot p \qquad (5)$$

depends on the bimolecular recombination rate constant B, and the electron and hole concentration. As quasi Fermi levels approach the band edges or V_{oc} increases, the charge carrier concentrations increase exponentially. At the same time, the mobility of charge carriers improves as more traps become filled. Improved mobility consequently increases the frequency of opposite charge carriers encountering each other at the interface, which enhances B for a diffusion limited recombination mechanism. Therefore the recombination rate is expected to increase with V_{oc}. Figure 7c depicts the plot of k_{rec} versus V_{oc} of different devices. The recombination rate was found to increase exponentially with bias, a characteristic that has been observed in DSSCs system.[23,41,62] For these TiO_2/P3HT devices, the slopes were found to be ~0.55 – 0.6 decade per 100 mV.

Most cells exhibit recombination rates of 10^3 - 10^5 s^{-1} at operating conditions. The right most point of each data set corresponds approximately to 1 sun intensity. Compared to the unmodified cell, all devices exhibit similar recombination rate constant curve shape (Fig. 7c). The same slopes suggest that interface modification has not altered the underlying recombination mechanism. Devices with earlier turn-on of dark current exhibit faster recombination rate as expected. The difference in the curves in Figure 7c can either be due to a translation along the V_{oc} axis, which is related to the changes in the effective Ec – HOMO gap, or a translation along the k_{rec} axis, which is related to the change in B. With the clear trend of how dipoles affects the V_{oc} (Sec. A), the main

contribution still comes from a shift in band edge offset at the TiO_2/polymer interface. The only exception is that the Z907 dye actually reduces the recombination rate because the alkyl chains form a charge carrier recombination barrier.

It is interesting that a layer of IMs does not have an effect on slowing down recombination, except Z907 with long alkyl chains. These results are similar to what was previously observed, that the IMs act more as an agent that modulates the interface energetics,[22] than as a recombination barrier. Researchers have investigated the use of a large bandgap inorganic material in DSSCs as charge transfer barriers.[41,71] The "monolayer" of IMs used here are less effective as recombination barrier probably due to imperfect coverage at the molecular scale or due to its π-conjugated semiconducting nature. It is also possible that the recombination across the TiO_2/P3HT interface is diffusion limited and a small alteration in the reaction rate has no effect on the recombination.

E. Optimized bilayer

Experimental results in earlier sections were obtained using a thick polymer layer so that the dark current could be more reproducible, and allowed analysis that assumes Beer's Law absorption. Here the characteristics of a bilayer cell was improved by optimizing layer thickness[14,66,72,73] to maximize the optical field close to the exciton splitting interface. This ensures a higher concentration of excitons is generated within a diffusion length away from the interface. Figure 8a shows the optical power profile at 532 nm wavelength (close to P3HT absorption maximum) inside a device stack with an optimum P3HT thickness of 50 nm. Figure 8b shows the J-V characteristics of actual

bilayer TiO_2/P3HT devices with three different IMs. Table II summarizes the device characteristics of these devices and the J_{sc} predicted based on L_d extracted from Figure 6a. As compared to earlier devices with thicker P3HT, the devices here typically exhibit ~1.5 times higher J_{sc}, while the V_{oc} is retained. The EQE of N3 modified devices was measured to be 19.5%, close to the estimated 20%. J_{sc} is highly reproducible to within ±10% and in devices with rectification ratios above 10^3 at -1V and 1 V, V_{oc} is consistent within ±15 mV. The power efficiency of some of these thin bilayer devices (or trilayer devices counting the IMs as a layer) approach 0.60 %.

IV. CONCLUSION

This work systematically studies the effect of interface modification in hybrid inorganic-organic PV cells and has provided insight to its device physics. It provides design strategy to improve this type of cell. We showed that both molecular dipoles and acid-base interaction can cause a band edge shift in TiO_2, resulting in a change in V_{oc}. This work illustrates that surface modification needs to take into account the effect of dipoles on the band edge shift, and the inevitable effects of protonation from carboxylic, phosphonic or sulfonic anchoring groups. We measured a larger L_d of P3HT of 6.5 – 8.5 nm on certain surface-modified TiO_2 compared to bare TiO_2, and showed that electron accepting nature of the IM is likely responsible for the photocurrent enhancement in PV devices. This larger L_d than previously thought has significant implications, for example, the dimensions of nanostructure in bulk-heterojunction PV cells needed for achieving efficient exciton harvesting may be relaxed. Utilizing the knowledge learned in this work, we increased the power efficiency of planar TiO_2/P3HT devices from 0.34 % to 0.6 %

with Ru(II) dye modifications. Z907 dye showed promises as the IM for use in bulk heterojunction nanostructured metal oxide-polymer PV cells due to its desirable properties of suppressing charge carrier recombination while retaining efficient exciton harvesting.

ACKNOWLEDGEMENTS

This work was supported by the Global Climate and Energy Project at Stanford University, the Department of Energy and a Kodak Research Fellowship. The authors would like to thank Colin Reese for simulating the dipole moments of the benzoic acid derivatives and Dr. Brian O'Regan for insightful discussions.

REFERENCES

[1]C. W. Tang, Appl. Phys. Lett. **48**, 183 (1986).

[2]G. Yu, J. Gao, J. C. Hummelen, F. Wudl, and A. J. Heeger, Science **270**, 1789 (1995).

[3]J. Halls, C. Walsh, N. Greenham, E. Marseglia, R. Friend, S. Moratti, and A. Holmes, Nature **376**, 498 (1995).

[4]W. Ma, C. Yang, X. Gong, K. Lee, and A. J. Heeger, Adv. Funct. Mater. **15**, 1617 (2005).

[5]F. Yang, M. Shtein, and S. R. Forrest, Nat. Mater. **4**, 37 (2005).

[6]G. Li, V. Shrotriya, J. S. Huang, Y. Yao, T. Moriarty, K. Emery, and Y. Yang, Nat. Mater. **4**, 864 (2005).

[7]S. E. Shaheen, D. S. Ginley, and G. E. Jabbour, MRS Bulletin **30**, 10 (2005).

[8]B. O'Regan, and M. Gratzel, Nature **353**, 737 (1991).

[9]U. Bach, D. Lupo, P. Comte, J. Moser, F. Weissortel, J. Salbeck, H. Spreitzer, and M. Gratzel, Nature **395**, 583 (1998).

[10]A. Hagfeldt, and M. Gratzel, Accounts Chem. Res. **33**, 269 (2000).

[11]B. Gregg, J. Phys. Chem. B **107**, 4688 (2003).

[12]I. G. Hill, A. Kahn, Z. G. Soos, and R. A. Pascal, Chem. Phys. Lett. **327**, 181 (2000).

[13]J. L. Bredas, J. Cornil, and A. J. Heeger, Adv. Mater. **8**, 447 (1996).

[14]L. A. A. Pettersson, L. S. Roman, and O. Inganas, J. Appl. Phys. **86**, 487 (1999).

[15]M. Theander, A. Yartsev, D. Zigmantas, V. Sundstrom, W. Mammo, M. Andersson, and O. Inganas, Phys. Rev. B **61**, 12957 (2000).

[16]J. Halls, K. Pichler, R. Friend, S. Moratti, and A. Holmes, Appl. Phys. Lett. **68**, 3120 (1996).

[17]J. E. Kroeze, T. J. Savenije, M. J. W. Vermeulen, and J. M. Warman, J Phys. Chem. B **107**, 7696 (2003).

[18]D. E. Markov, E. Amsterdam, P. W. M. Blom, A. B. Sieval, and J. C. Hummelen, J. Phys. Chem. A **109**, 5266 (2005).

[19]P. Peumans, and S. R. Forrest, Chem. Phys. Lett. **398**, 27 (2004).

[20]V. D. Mihailetchi, L. J. A. Koster, J. C. Hummelen, and P. W. M. Blom, Phys. Rev. Lett. **93**, 216601 (2004).

[21]T. Offermans, S. C. J. Meskers, and R. A. J. Janssen, Chem. Phys. **308**, 125 (2005).

[22]J. Kruger, U. Bach, and M. Gratzel, Adv. Mater. **12**, 447 (2000).

[23]J. R. Durrant, S. A. Haque, and E. Palomares, Coord. Chem. Rev. **248**, 1247 (2004).

[24]Y. X. Liu, S. R. Scully, M. D. McGehee, J. S. Liu, C. K. Luscombe, J. M. J. Frechet, S. E. Shaheen, and D. S. Ginley, J Phys. Chem. B **110**, 3257 (2006).

[25]J. Moser, S. Punchihewa, P. P. Infelta, and M. Gratzel, Langmuir **7**, 3012 (1991).

[26]R. Cohen, L. Kronik, A. Shanzer, D. Cahen, A. Liu, Y. Rosenwaks, J. K. Lorenz, and A. B. Ellis, J. Am. Chem. Soc. **121**, 10545 (1999).

[27]R. J. Kline, M. D. Mcgehee, and M. F. Toney, Nat. Mater. **5**, 222 (2006).

[28]A. Salleo, M. L. Chabinyc, M. S. Yang, and R. A. Street, Appl. Phys. Lett. **81**, 4383 (2002).

[29]Y. X. Liu, M. A. Summers, C. Edder, J. M. J. Frechet, and M. D. McGehee, Adv. Mater. **17**, 2960 (2005).

[30]P. A. van Hal, M. P. T. Christiaans, M. M. Wienk, J. M. Kroon, and R. A. J. Janssen, J. Phys. Chem. B **103**, 4352 (1999).

[31]P. van Hal, M. Wienk, J. Kroon, W. Verhees, L. Slooff, W. van Gennip, P. Jonkheijm, and R. Janssen, Adv. Mater. **15**, 118 (2003).

[32]W. J. E. Beek, M. M. Wienk, and R. A. J. Janssen, Adv. Mater. **16**, 1009 (2004).

[33]A. Arango, L. Johnson, V. Bliznyuk, Z. Schlesinger, S. Carter, and H. Horhold, Adv. Mater. **12**, 1689 (2000).

[34]K. M. Coakley, Y. X. Liu, M. D. McGehee, K. L. Frindell, and G. D. Stucky, Adv. Funct. Mater. **13**, 301 (2003).

[35]K. M. Coakley, and M. D. McGehee, Appl. Phys. Lett. **83**, 3380 (2003).

[36]K. M. Coakley, and M. D. McGehee, Chem. Mater. **16**, 4533 (2004).

[37]C. Goh, K. M. Coakley, and M. D. McGehee, Nano Lett. **5**, 1545 (2005).

[38]P. Ravirajan, A. M. Peiro, M. K. Nazeeruddin, M. Graetzel, D. D. C. Bradley, J. R. Durrant, and J. Nelson, J. Phys. Chem. B **110**, 7635 (2006).

[39]D. C. Olson, J. Piris, R. T. Collins, S. E. Shaheen, and D. S. Ginley, Thin Solid Films **496**, 26 (2006).

[40]G. Ashkenasy, D. Cahen, R. Cohen, A. Shanzer, and A. Vilan, Accounts Chem. Res. **35**, 121 (2002).

[41]B. C. O'Regan, S. Scully, A. C. Mayer, E. Palomares, and J. Durrant, J. Phys. Chem. B **109**, 4616 (2005).

[42]T. Stubinger, and W. Brutting, J. Appl. Phys. **90**, 3632 (2001).

[43]C. Goh, R. J. Kline, M. D. McGehee, E. N. Kadnikova, and J. M. J. Frechet, Appl. Phys. Lett. **86**, 122110 (2005).

[44]F. Nuesch, M. Carrara, and L. Zuppiroli, Langmuir **19**, 4871 (2003).

[45]S. Ruhle, M. Greenshtein, S. G. Chen, A. Merson, H. Pizem, C. S. Sukenik, D. Cahen, and A. Zaban, J Phys. Chem. B **109**, 18907 (2005).

[46]M. K. Nazeeruddin, S. M. Zakeeruddin, R. Humphry-Baker, M. Jirousek, P. Liska, N. Vlachopoulos, V. Shklover, C. H. Fischer, and M. Gratzel, Inorg. Chem. **38**, 6298 (1999).

[47]P. Wang, S. M. Zakeeruddin, J. E. Moser, M. K. Nazeeruddin, T. Sekiguchi, and M. Gratzel, Nat. Mater. **2**, 402 (2003).

[48]G. Rothenberger, D. Fitzmaurice, and M. Gratzel, J. Phys. Chem. **96**, 5983 (1992).

[49]L. Zuppiroli, L. Si-Ahmed, K. Kamaras, F. Nuesch, M. N. Bussac, D. Ades, A. Siove, E. Moons, and M. Gratzel, Eur. Phys. J. B **11**, 505 (1999).

[50]S. Khodabakhsh, D. Poplavskyy, S. Heutz, J. Nelson, D. D. C. Bradley, F. Murata, and T. S. Jones, Adv. Funct. Mater. **14**, 1205 (2004).

[51]B. de Boer, A. Hadipour, M. M. Mandoc, T. van Woudenbergh, and P. W. M. Blom, Adv. Mater. **17**, 621 (2005).

[52]D. R. Lide, Ed. (2006). CRC Handbook of Chemistry and Physics. Boca Raton, Taylor and Francis.

[53]simulated using density functional theory with 6-311++Gdp basis set

[54]J. A. Barker, C. M. Ramsdale, and N. C. Greenham, Phys. Rev. B **67**, 075205 (2003).

[55]T. F. Heinz, H. W. K. Tom, and Y. R. Shen, Phys. Rev. A **28**, 1883 (1983).

[56]J. A. Harrison, and D. W. Shoesmit*, J. of Electroanal. Chem. **32**, 125 (1971).

[57]J. Weber, and J. Volke, Electrochim. Acta **24**, 113 (1979).

[58]E. D. Clarke, P. Wardman, and K. H. Goulding, Biochemical Pharmacology **29**, 2684 (1980).

[59]A. Hagfeldt, and M. Gratzel, Chem. Rev. **95**, 49 (1995).

[60]G. P. Bartholomew, and A. J. Heeger, Adv. Funct. Mater. **15**, 677 (2005).

[61]L. Schmidt-Mende, J. E. Kroeze, J. R. Durrant, M. K. Nazeeruddin, and M. Gratzel, Nano Lett. **5**, 1315 (2005).

[62]S. A. Haque, Y. Tachibana, R. L. Willis, J. E. Moser, M. Gratzel, D. R. Klug, and J. R. Durrant, J. Phys. Chem. B **104**, 538 (2000).

[63]M. K. Nazeeruddin, A. Kay, I. Rodicio, R. Humphrybaker, E. Muller, P. Liska, N. Vlachopoulos, and M. Gratzel, J. Am. Chem. Soc. **115**, 6382 (1993).

[64]B. A. Gregg, J. Sprague, and M. W. Peterson, J. Phys. Chem. B **101**, 5362 (1997).

[65]S. Scully, and M. D. McGehee, J. Appl. Phys. **100**, 034907 (2006).

[66]P. Peumans, A. Yakimov, and S. R. Forrest, J. Appl. Phys. **93**, 3693 (2003).

[67]I. D. W. Samuel , MRS Fall Meeting (2005).

[68]obtained by first solving the continuity equation for a TiO2/thick polymer bilayer geometry assuming exciton diffusion length of Ld and Beer's law generation rate profile, and then by taking the slope of the steady state exciton concentration profile at the TiO2/polymer interface, which gives the photocurrent density. EQE is the photocurrent density divided by the incident photon flux. .

[69]N. A. Anderson, E. C. Hao, X. Ai, G. Hastings, and T. Q. Lian, Chem. Phys. Lett. **347**, 304 (2001).

[70]W. J. E. Beek, and R. A. J. Janssen, Adv. Funct. Mater. **12**, 519 (2002).

[71]E. Palomares, J. N. Clifford, S. A. Haque, T. Lutz, and J. R. Durrant, J. Am. Chem. Soc. **125**, 475 (2003).

[72]P. Ravirajan, S. Haque, J. Durrant, D. Poplavskyy, D. Bradley, and J. Nelson, J. Appl. Phys. **95**, 1473 (2004).

[73]P. Ravirajan, S. A. Haque, D. Poplavskyy, J. R. Durrant, D. D. C. Bradley, and J. Nelson, Thin Solid Films **451/452**, 624 (2004).

Table

TABLE I. CRC values of dipole moments (D) of substituted benzene without the carboxylic groups and dipole moments simulated for the full benzoic acid derivative structure using density functional theory (DFT).

Subtituted Group	CRC	DFT
$-SO_2F$	-	4.5
$-NO_2$	4.2	3.8
-CN	4.0	3.4
-Br	1.7	1.4
-H	0	-2.1
$-OCH_3$	-1.4	-3.9
$-NH_2$	-1.1	-4.5

TABLE II. Tabulated device characteristics of devices shown in Figure 8c. The last column shows the J_{sc} predicted by modeling using L_d extracted from Figure 6a.

Devices	J_{sc} (mA/cm^2)	V_{oc} (V)	FF	η (%)	Estimated J_{sc} (mA/cm^2)
Unmodified	0.85	0.60	0.67	0.34	0.80
-NO2	1.40	0.51	0.62	0.44	1.56
Z907	1.21	0.67	0.69	0.56	-
N3 + TBP	1.86	0.57	0.57	0.60	1.92

Figure Captions

FIG. 1. (a) Schematic of bilayer TiO_2/polymer devices with dipolar modification of titania surface. The table lists the substituent –R group on the para position of the benzoic acid accompanied with calculated dipole moment. (b) Molecular structures of the benzene carboxylic molecules with varying amount of carboxylic acid groups. (c) Molecular structures of the three Ru(II) dyes as IM.

FIG. 2. Schematics of band diagram of TiO_2/polymer cell at flat band (assumed to be close to open circuit condition) (a) with interfacial dipoles pointing towards TiO_2, (b) without any modification (c) with interfacial dipoles pointing away from TiO_2. Quasi Fermi levels are drawn as dash lines and the split between them dictates the V_{oc}.

FIG. 3. J-V curves of TiO_2/160 nm P3HT bilayer devices with and without interface modifications employing para-substituted benzoic acid derivatives (a) in dark and (b) under illuminations. (c) V_{oc} and J_{sc} of devices shown in **b** plotted against dipole moment of the modifiers. A dashed line is drawn as a guide to the eye.

FIG. 4. J-V curves of TiO_2/160 nm P3HT bilayer devices with and without interface modifications employing multiply substituted benzene carboxylic acid molecules (a) in dark and (b) under illuminations.

FIG. 5. J-V curves of planar TiO_2/160 nm P3HT cells with and without interface modifications using Ru(II) dyes (a) in dark and (b) under illuminations. (c) Photocurrent action spectra of devices in **b** showing contribution to photocurrent enhancement only originates from P3HT absorption upon interface modifications with Ru dyes.

FIG. 6. (a) PL quenching efficiency of P3HT on surface modified TiO_2 versus polymer thickness. Lines are fit using Equation 2 with different L_d. (b) EQE at an excitation wavelength of 512 nm with a power intensity of 1.7 mW/cm^2 as a function of applied voltage of bilayer TiO_2/160 nm P3HT devices with and without titania surface modification.

FIG. 7. (a) Schematic of a band diagram of TiO_2/polymer cell in a transient photovoltage measurement setup. The devices are held at open circuit condition while under illumination by a bias lamp, which sets the open circuit voltage magnitude. A pulsed light is introduced to create a transient photovoltage, which decays as these charge carriers recombine with certain recombination lifetime. (b) A typical photovoltage transient, which can be fit to a monoexponential decay function as shown in the log-linear plot in inset. (c) k_{rec} versus V_{oc} measured for bilayer TiO_2/160 nm P3HT device with and without various surface modification.

FIG. 8. (a) Optical power profile at 532 nm wavelength in the glass/FTO/TiO_2/P3HT/Ag device stack. J-V characteristics of optimized bilayer devices employing thin (50 nm) polymer layer (b) in dark and (c) under illuminations.

(a)

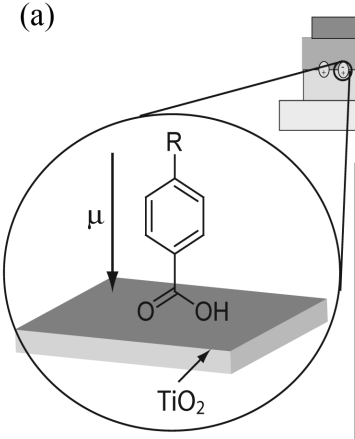

-R Group	Dipole Moment (D)
-SO_2F	4.5
-NO_2	3.8
-CN	3.4
-Br	1.4
-H	-2.1
-OCH_3	-3.9
-NH_2	-4.5

(b)

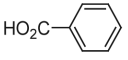

MONO-carboxylic
(-**H** or benzoic acid)

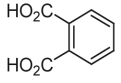

DI-carboxylic

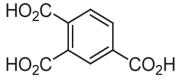

TRI-carboxylic

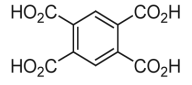

TETRA-carboxylic

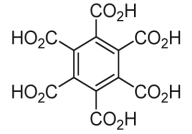

HEXA-carboxylic

(c)

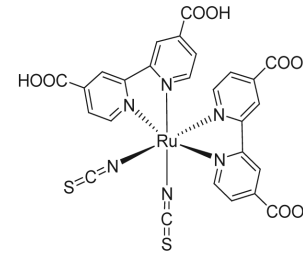

N3

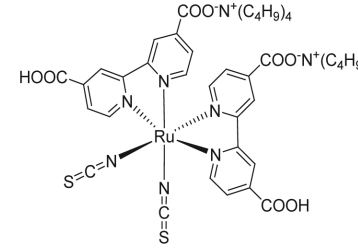

N719

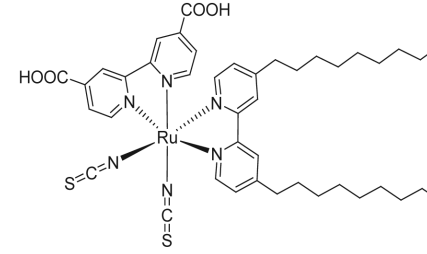

Z907

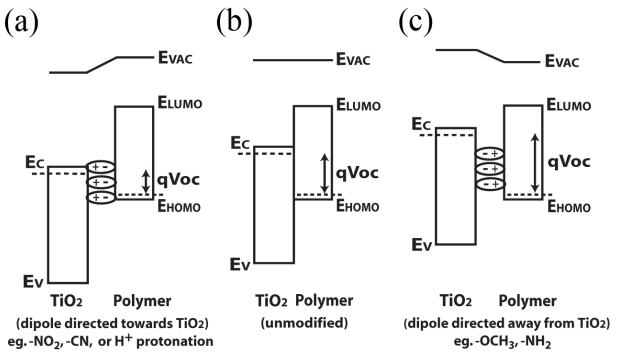
(a)
EVAC
ELUMO
EC
qVoc
EHOMO
EV
TiO2 Polymer
(dipole directed towards TiO2)
eg. -NO2, -CN, or H+ protonation
(b)
EVAC
ELUMO
EC
qVoc
EHOMO
EV
TiO2 Polymer
(unmodified)
(c)
EVAC
ELUMO
EC
qVoc
EHOMO
EV
TiO2 Polymer
(dipole directed away from TiO2)
eg. -OCH3, -NH2

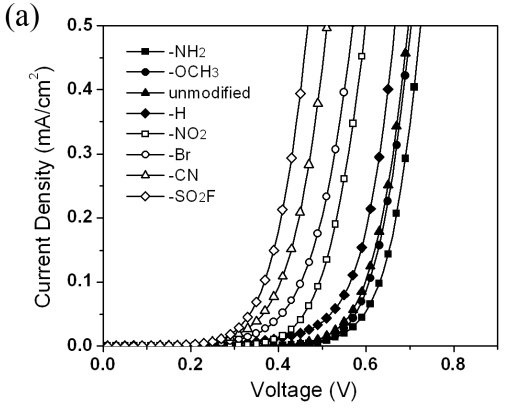
(a)
Current Density (mA/cm2)
Voltage (V)
-NH2
-OCH3
unmodified
-H
-NO2
-Br
-CN
-SO2F

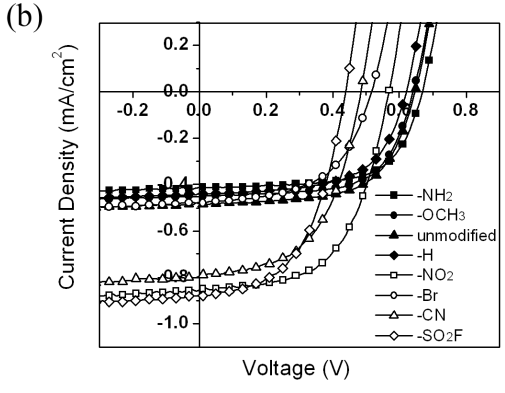
(b)
Current Density (mA/cm2)
Voltage (V)
-NH2
-OCH3
unmodified
-H
-NO2
-Br
-CN
-SO2F

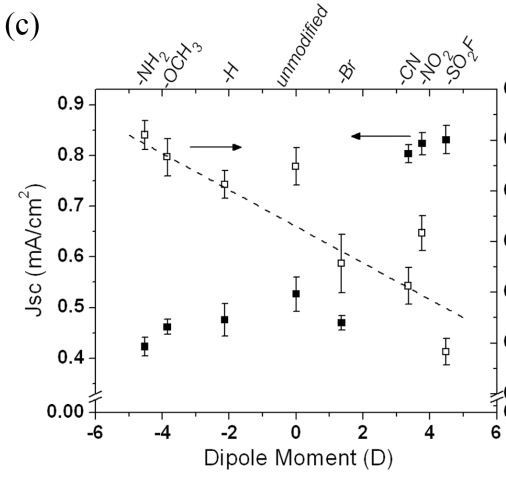
(c)
-NH2
-OCH3
-H
unmodified
-Br
-CN
-NO2
-SO2F
Jsc (mA/cm2)
Voc (V)
Dipole Moment (D)

(a)

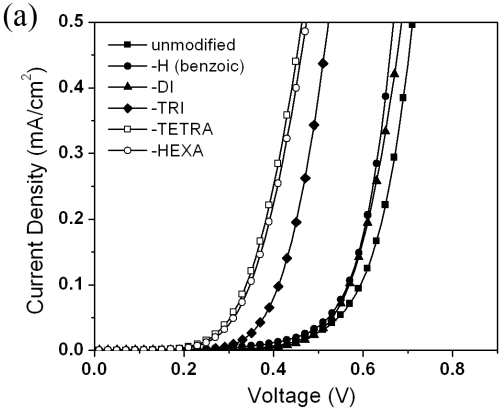
Current Density (mA/cm^2)
Voltage (V)
unmodified
-H (benzoic)
-DI
-TRI
-TETRA
-HEXA
0.0
0.1
0.2
0.3
0.4
0.5
0.6
0.8

(b)

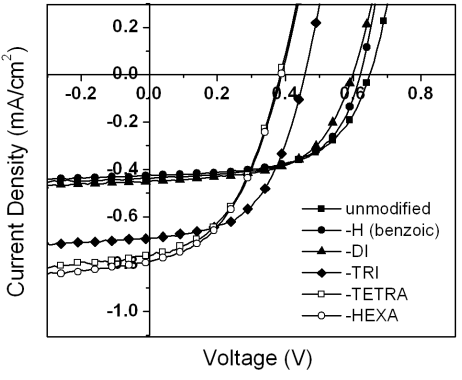
Current Density (mA/cm^2)
Voltage (V)
unmodified
-H (benzoic)
-DI
-TRI
-TETRA
-HEXA
-0.2
0.0
0.2
0.4
0.6
0.8
-1.0

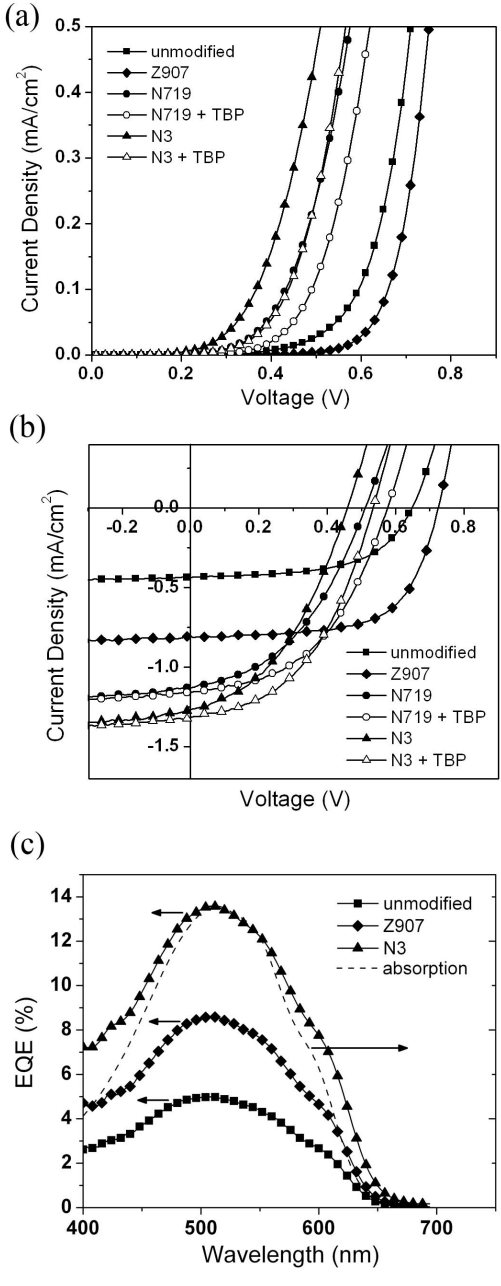
(a)
Current Density (mA/cm^2)
Voltage (V)
unmodified
Z907
N719
N719 + TBP
N3
N3 + TBP
(b)
Current Density (mA/cm^2)
Voltage (V)
unmodified
Z907
N719
N719 + TBP
N3
N3 + TBP
(c)
EQE (%)
Optical Density
Wavelength (nm)
unmodified
Z907
N3
absorption

(a)

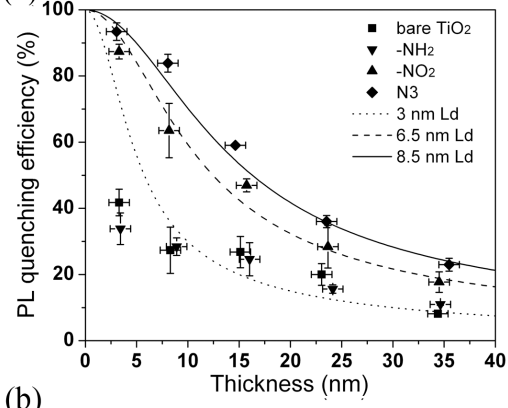
PL quenching efficiency (%)
Thickness (nm)
bare TiO2
-NH2
-NO2
N3
3 nm Ld
6.5 nm Ld
8.5 nm Ld

(b)

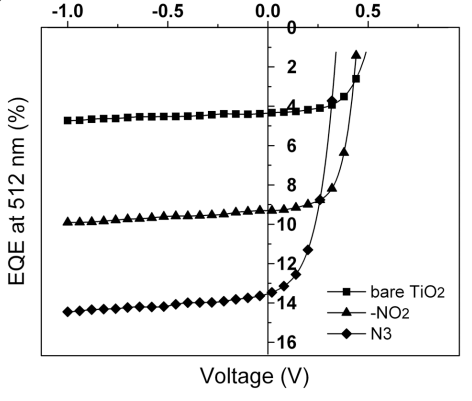
EQE at 512 nm (%)
Voltage (V)
bare TiO2
-NO2
N3

(a)

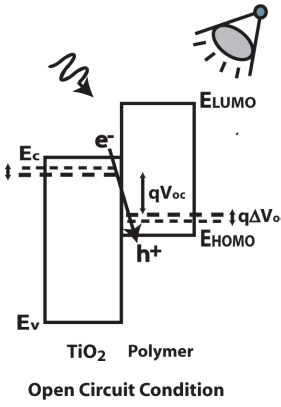

Open Circuit Condition

(b)

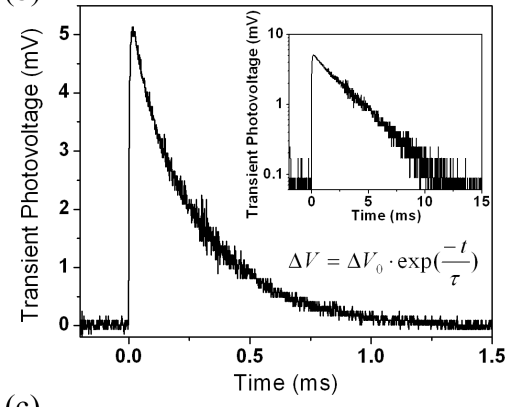

(c)

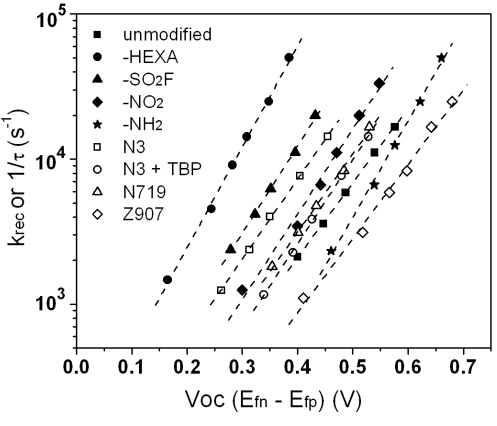

(a)

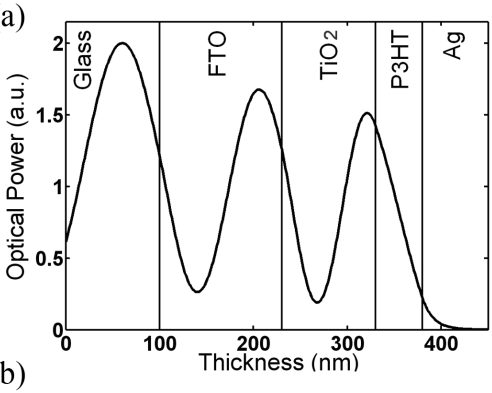
Glass
FTO
TiO2
P3HT
Ag
Optical Power (a.u.)
Thickness (nm)
0
0.5
1
1.5
2
0
100
200
300
400

(b)

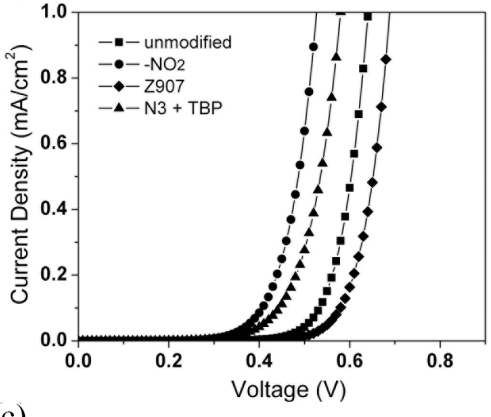
unmodified
-NO2
Z907
N3 + TBP
Current Density (mA/cm2)
Voltage (V)
0.0
0.2
0.4
0.6
0.8
1.0

(c)

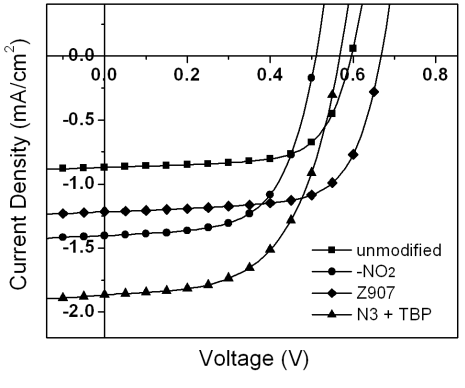
unmodified
-NO2
Z907
N3 + TBP
Current Density (mA/cm2)
Voltage (V)
0.0
-0.5
-1.0
-1.5
-2.0
0.0
0.2
0.4
0.6
0.8